Structural Load Alleviation using Distributed Delay Shaper: Application to Flexible Aircraft

Mushfiqul Alam[a,b], Martin Hromcik[a]

[a] *Faculty of Electrical Engineering, Czech Technical University in Prague, Czech Republic; Email: mushfala@fel.cvut.cz or malam@liverpool.ac.uk*
[b] *The University of Liverpool, School of Engineering, Liverpool, United Kingdom*

Abstract

Lightweight flexible aircraft suffers from unwanted oscillatory vibrations during aircraft manoeuvres. A recently developed distributed-delay signal (DZV) shaper is therefore proposed to be applied as a feedforward controller to alleviate the manoeuvre loads, as an alternative to traditional structural filters used routinely in this context. Structural filters are essentially linear low-pass filters with bandwidth below the significant flexible modes, applied to control signals generated either by the pilot's direct input or by the flight control system. It has been showed that if instead a properly tuned signal shaper is used, better performance can be achieved: first, the target modes are significantly attenuated while the responsiveness of the aircraft is less compromised and secondly, the oscillatory nature of the vibrations are reduced. The high fidelity simulation results on a full scaled dynamic model of a highly flexible blended wing body (BWB) aircraft show that in comparison to traditional structural filters, signal shapers significantly reduce the wing root loading (forces and moments) which provides potential structural benefits.

Keywords:
signal shaper, flexible aircraft, feedforward controller, load alleviation, input shaper, flight control

1. Introduction

Signal shaping is a renowned method for compensating the undesirable oscillatory motions of various flexible mechanical systems. Broadly speaking, signal shaper works by creating a command signal that cancels its own vibration. That is, vibration caused by the first portion of the command signal (in time domain) is cancelled by vibrations induced by the rest of the command. If designed correctly, the shaped command used to drive the system will result in reduced vibrations with respect to the reference command. Signal shapers (PosiCast, zero vibration (ZV), ZV derivative (ZVD), extra insensitive (EI), etc.) have been in the centre of attention for decades as an efficient feedforward control tool for manipulation of oscillatory systems, like large cranes, lightweight (therefore, flexible) manipulators, or mechanical structures (M. Smith (1957); Singhose et al. (1996); Singer and Seering (1990)) and most recently by Cole et al. (2018). Next to classical lumped-delay, shapers such as ZV, ZVD, distributed-delay shapers (the DZV shaper, as an example seeVyhlídal et al. (2013a)) with interesting spectral and sensitivity properties are proposed recently (Vyhlídal and Hromčík (2015); Vyhlídal et al. (2016); Alikoç et al. (2016)). The smoothers exhibit slightly improved residual vibration characteristics at higher frequency; precisely retarded distribution of the spectrum of zeros are the main benefits of DZV shaper (Alikoç et al. (2016)).

Recent developments of the light weight aircraft have led to flexible aircraft with pronounced aeroelastic effects. In flight control application, pilot's input command to a control surface often excites the flexible modes of the aircraft causing unwanted oscillatory vibrations at the wing root with large values of elastic displacement and acceleration in addition to those components of displacement and acceleration which arise from the rigid body motion of the aircraft. The interaction between an aircraft's structural dynamics, unsteady aerodynamics and flight control system is known as aeroservoelasticity (R. Taylor, R. Pratt (1996)). In the case of flexible aircraft, responses of the elastic motion are comparable to that of the rigid body motion, this similarity/coupling of the rigid body energy and the elastic energy leads to deterioration of the flying qualities of the aircraft (McLean (1990); Stevens et al. (2015)). These aeroelastic behaviour of the aircraft are required to be taken into account during control law design (Tuzcu (1999); Su and S. Cesnik (2010)). The problem is that the control system's sensors are of sufficient bandwidth to sense the structural vibrations as well as the rigid-body motion of the aircraft. Therefore special attention is necessary while designing the flight control system for this coupled rigid-body and aeroelastic dynamics.

Aeroservoelastic filtering is a traditional method for suppressing elastic modes, but this usually comes at an expense in terms of reducing the phase margin in a flight control system (Pratt et al. (1994)). If the phase margin is significantly reduced, aircraft responses may become insensitive to pilot commands. Consequently, with a phase lag in the control inputs, potential pilot induced oscillations (PIOs) can occur. "Structural filters" such as linear low-pass Butterworth, Bessel or other-type filters are traditionally used as a clever feedforward control solution to pilot's input command to the stability augmented flight control system (SAFCS) for attenuating/damping (so as to reduce excitation) of the flexible modes (R. Taylor, R. Pratt (1996); Elliott (1987)). Miller (2011) at NASA documented some form of the use of structural filters to attenuate the structural vibrations. Another alternative to low-pass "Structural filters" is notch filters. Notch filters are generally usedused in feedback architecture to damp the flexible modes of the aircraft, see for example Hoogendijk et al. (2014); Oh et al. (2008). Additionally, other types of multivaraible feedback controllers such as $\mathcal{H}_\infty$ has been developed for manoeuvre load reduction (Burlion et al. (2014); Torralba et al. (2009)). The limitation of the feedback load alleviation controllers are that they purely depend on the error feedback, hence the maximum value of 1st peak of the forces and moments at the wing root can not be reduced (Alam et al. (2015)).

The excitation of the flexible modes causes high magnitude oscillatory forces and moments at the wing root joint of the aircraft. These oscillatory high magnitude forces and moments at the wing root joint results in reduction of the structural life of the airframe due to the large dynamic loads and the resultant high levels of stress. What is of the most importance are the maximum value of the peaks and oscillatory nature of the forces and moments at wing root joints. These peak values and oscillatory nature of the wing root joint loading (forces and moments) determines the prediction of the fatigue failures of the airframe.

In comparison to traditional low-pass filters and notch filters in feedforward architecture, signal shapers are a strong candidate for inclusion into SAFCS for flexible aircraft. Signal shaper can be regarded as an add-on feedforward controller to a already functioning SAFCS. Flexible aircraft typically features hull and wing bending. A properly tuned signal shapers targeted at the most prominent flexible modes of the aircraft can lead to superior responsiveness and more efficient reduction of unwanted oscillations in the forces and moments at wing root joints (Singhose et al. (1994)).

This paper aims at providing a detailed analysis on the use of signal shapers, namely DZV as an alternative to widely used traditional low-pass filters (Butterworth and Bessel) and notch filter as a feedforward solution to the SAFCS of a flexible aircraft and the results on reducing the vibration impacts on the aircraft with respect to wing root forces and moments. As a case study, we present the results of a pilot's push-pull command (which is regarded as a standard manoeuvre for flight tests in the aerospace industry) using the elevator deflection on a full scale industry quality dynamic model of a highly flexible blended-wing-body (BWB) aircraft provided by the ACFA2020 consortium under the European Union's FP7 Research Framework. It has been shown that using a properly tuned DZV controller better reduction in dynamic loads are possible compared to traditional low-pass filters which can increase the structural lifetime of the aircraft.

Nevertheless, the principles demonstrated with the DZV controller can be used for the existing flexible tube-wing configuration aircraft such as Boeing 787 Dreamliner or Airbus A350 XWB. Thus the novelty in this paper lies in proposing DZV controller as feedforward controller to the SAFCS of the flexible aircraft as an alternative to the traditional low-pass filters (Butterworth, Bessel, etc.) and notch filter which will efficiently alleviate the wing root loading.

The rest of the paper is organized as follows: Section 2 presents the fundamental features of the DZV shaper. Section 3 presents a discussion on the aircraft's dynamic model. Section 4 describes in detail the design of the signal shaper and control law. Section 5 provides a detailed analysis on the performance improvement due to the DZV shaper inclusion. Section 6 contains final concluding remarks.

2. Zero vibration shapers with lumped and distributed delays

A general form of a zero vibration shaper is written as follows:

$$u(t) = Aw(t) + (1-A)\int_0^{\vartheta} w(t-\eta)dh(\eta). \tag{1}$$

Here w and u are the shaper input and output, respectively. The parameters are the gain $A \in [0,1]$ and the time delay with a shape determined by $h(\eta)$. Here $h(\eta)$ is a non-decreasing function over the interval $\eta \in [0,\vartheta]$ with the boundary values $h(0) = 0$ and $h(\vartheta) = 1$. The transfer function of the shaper is therefore given by:

$$S(s) = A + (1-A)\Gamma(s). \tag{2}$$

Here $\Gamma(s) = L\{g(\eta)\}$, with $g(\eta) = \frac{dh(\eta)}{d\eta}$ being the impulse response of the delay. The zeros of shaper (2) are determined as the roots of the equation $S(s) = 0$.

The most common shaper is zero vibration shaper (Singer and Seering (1990); Singhose et al. (1994)), and is denote as ZV. The ZV shaper includes a lumped delay in the following form:

$$\Gamma(s) = e^{-sT}, \tag{3}$$

in the shaper transfer function (2). The parameters such as A and T of the classical ZV shaper are given as following:

$$A = \frac{e^{\frac{\beta}{\Omega}\pi}}{1 + e^{\frac{\beta}{\Omega}\pi}}, T = \frac{\pi}{\Omega}. \tag{4}$$

And the equation of the shaper's zeros are given as following:

$$s_{2k+1,2k+2} = -\frac{1}{T} ln \frac{A}{1-A} \pm j\frac{\pi}{T}(2k+1), k = 0, 1, ..., \infty. \tag{5}$$

It can be noticed, the spectrum of the shaper is composed with the neutral chain of infinite number of zeros with the identical real part and periodically decreasing/increasing imaginary parts. From these infinitely many zeros, only the dominant pair $s_{1,2} = -\frac{1}{T} ln \frac{A}{1-A} \pm j\frac{\pi}{T}$ is used to compensate the pole of the system $r_{1,2}$ (M. Smith (1957)).

As an example of distributed delays shaper, we adopted the $D^\alpha ZV$ shaper class with shaper delay defined by:

$$\Gamma(s) = \frac{1}{(1-\alpha)T} \frac{e^{-s\alpha T} - e^{-sT}}{s}, \tag{6}$$

in the shaper transfer function (2), proposed earlier by the authors in (Vyhlídal et al. (2013b)). The delay is based in this case on a weighted connection of one lumped and one equally distributed delay. The parameter T represents the overall delay length, $T \in R^+$, and $\alpha \in (0, 1)$ determines the ratio between the length of the lumped delay and the overall delay T. Note that for $\alpha \to 1$ one gets the classical ZV shaper. And for $\alpha = 0$ we get the so called DZV shaper with a pure equally distributed delay (Vyhlídal et al. (2013a)). Due to increased complexity of the characteristic equation $S(s) = 0$, the $D^\alpha ZV$ shaper parametrization is not as straightforward as for the case of ZV shaper.

In Vyhlídal et al. (2013b), a numerical parametrization procedure has been designed. Recently, fully analytical approach has been proposed in Vyhlídal and Hromčík (2015). For providing information to the reader on the parameter ranges, the design graphs for various values of α is presented in Fig. 1, which is adopted from Vyhlídal et al. (2013b).

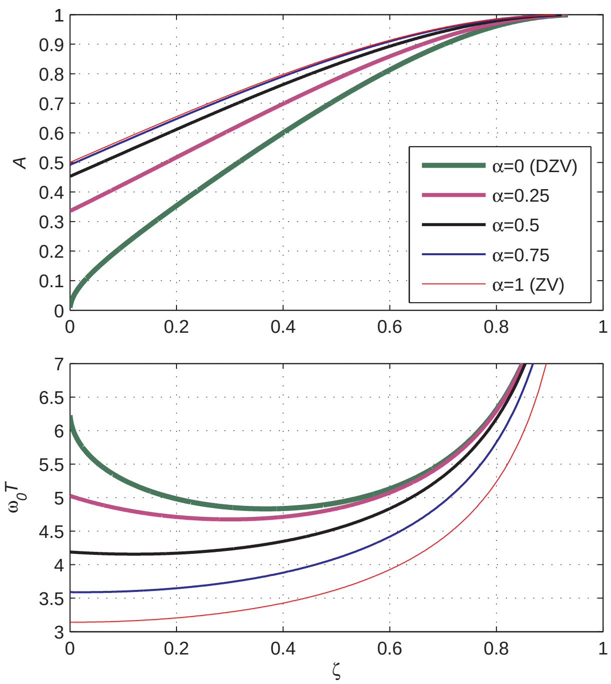

Figure 1: Parametrization of shapers $D^{\alpha}ZV$ for $\alpha = 0, 0.25, 0.5, 0.75$ and 1 (ZV shaper). Adopted from Vyhlídal et al. (2013a).

Note that the gain parameter A depends on the damping ratio ζ and the parameter α determining the delay composition. The delay parameter T depends on ζ and the parameter α and additionally, on the natural frequency ω_0. It can be seen in Fig. 1, the largest differences in the parameters appear for the small values of ζ. Notice that for $\zeta = 0$ the normalized delay $T\omega_0$, and the gain A vary from $T\omega_0 = \pi$ and $A = 0.5$ for ZV to $T\omega_0 = 2\pi$ and $A = 0$ for D^0ZV (in fact DZV) shaper. With increasing ζ, the differences between the parameters for different types of shapers are getting smaller. It is worth mentioning, an important feature of both types of shapers is that for $\alpha \geq 0.5$, their gain values A are fairly close to each other over the whole range of ζ. Let us mention that all the types of shapers have the same limits for $\zeta \to 1$, for which $A \to 1$ and $T\omega_0 \to \infty$.

Practically, for the given damping ratio ζ and the selected parameter α, the gain A and the normalized delay $T\omega_0$ can be obtained from the tabulated data shown in Fig. 1. Let us remark that the parametrization of the shapers is available in the form of MATLAB functions[1].

It is important to note here that, one could be interested whether equally good oscillation suppression schemes could be achieved by more conventional approaches instead of input shaping: namely by using a (finite-dimensional) notch filter or a low-pass filter. The answer to this question is no. For the low-pass filters, the reasoning is analogous to the comparison between the input shapers and the input smoothers performed in Singhose et al. (2010). As demonstrated, even though the smoothers slow down the system response, the oscillations at the flexible part are still being excited, even though their amplitude is smaller. The notch filters on the other hand give rise to disadvantageous transients; while the DZV shaper feature *monotonic* and simple piecewise constant or linear step responses, the step response of a related second-order notch filter represents a *nonmonotonic* and comparatively complex motion. From the frequency-domain and zero-pole-cancellation perspectives though, performance of the zero-vibration shapers and a notch filter is analogous. For comparison of shaper-based and shaper-free architectures for flexible mode compensation see also a recent work Pilbauer et al. (2016); Hromčík and Vyhlídal (2017).

3. Dynamic Modeling

Several European research initiatives were taken for the development of efficient light weight future generation commercial aircraft through projects such as ACFA (Active Control for Flexible Aircraft) 2020, NACRE (New Aircraft Concepts Research), VELA (Very Efficient Light Aircraft) and ROSAS (Research on Silent Aircraft Concepts), details about these projects can be found in (Cambier and Kroll (2008); ACFA (2008); Frota (2010); Hepperle (2005)). RSOAS proposed the preliminary concept of blended wing

[1] http://www.cak.fs.cvut.cz/algorithms/shapers

body (BWB) configuration as the the future generation aircraft. VELA and NACRE were dedicated for the conceptualization, development, optimization, numerical and experimental validation of a BWB aircraft configuration. The major targets for improved aircraft efficiency with respect to the fuel consumption and external noise reduction was achieved within the preliminary design of a 450 passenger BWB aircraft through ACFA2020 project. ACFA2020 further studied the implementation of robust, adaptive multi input-multi output (MIMO) control, model reduction techniques along with various other control architectures for loads alleviation, improvement in passenger's ride comfort and flight handling qualities of BWB type aircraft (Kozek and Schirrer (2015)). As part of the main goals of the project, the aircraft's aeroelastic properties were explicitly analysed with respect to modern control design techniques. The finalized dynamic models were generated based on a refined Finite Element Model (FEM) and aerodynamic data (Kozek and Schirrer (2015)) for carrying out load analysis and control law design.

The aircraft's dynamic model used for loads analysis, design and validation of the DZV controller is based on aerodynamic and structural data of the NACRE BWB configuration developed within the European research projects, namely, NACRE and ACFA2020 (Kozek and Schirrer (2015); Alam et al. (2015); Alam (2014)). The original aircraft model was not developed for dynamic load analysis. In order to perform dynamic load analysis essential modifications were made to the aircraft. Structural components such as cockpit, elevator, wing's leading edge and engine pylon were added as concentrated point masses (Kozek and Schirrer (2015)). Non-structural masses of systems, equipment, operational masses, different passenger/payloads and fuel configurations were incorporated into the structural model of the NACRE BWB configuration (Frota (2010)), see Fig. 2.

Aerodynamic and flight dynamic parameters (such as damping derivatives, control surface derivatives, etc.) were provided by the NACRE project for various mass cases and cruise speeds. For the analysis seven different mass cases as a fraction of full fuel loads are considered as listed in Table 1.

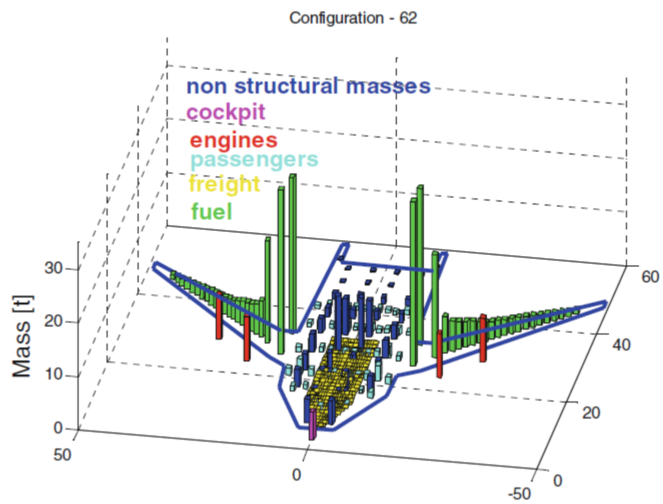

Figure 2: Distribution of non-structural masses in NACRE BWB aircraft (Kozek and Schirrer (2015); Wildschek et al. (2010)).

Table 1: Mass case variations.

Fuel (as fraction of full mass)	0	1/16	1/8	1/4	1/2	3/4	1
No. Mass Case	1	2	3	4	5	6	7

The analysis focused on the short period mode of the longitudinal flight dynamics. The longitudinal motion of the NACRE BWB aircraft was statically unstable across large regions of mass and flight envelopes, see Fig. 3a. Therefore, artificial longitudinal flight stabilization was provided by a simple alpha-feedback control law into the elevator channel to stabilize the aircraft, see Fig 3b. The original NACRE longitudinal dynamic model consisted of 20 states in total including the rigid body and flexible modes.

3.1. Computation of Static Wing Loads

In order to compute the structural load at $1g$ level flight the aircraft's finite element model (FEM) is loaded by gravitational forces as well as aerodynamic forces that were computed by trim analysis for $1g$ level flight. Using the estimated loads, cut forces and moments were evaluated at the wing root, see Fig 4.

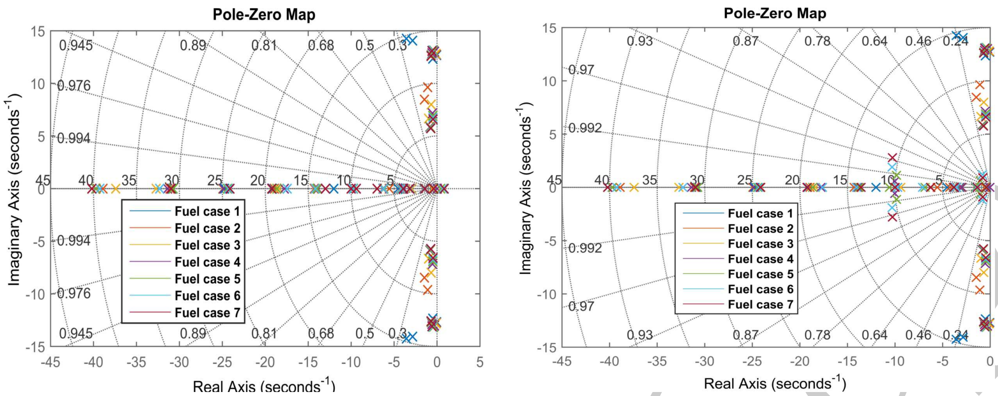

(a) Unstable original aircraft (b) Stabilized aircraft with alpha feedback.

Figure 3: Pole-zero plot of the NACRE-BWB aircraft.

3.2. Aerodynamics

Mass-normalised mode shapes ($\mathbf{\Phi}$) of the unconstrained structure are computed by modal decomposition. Unsteady aerodynamic forces are projected to this set of degrees of freedom (DOF). Rigid body modes for aerodynamic forces in flight dynamics, are normalized to displacements of $1m$ for translational modes, respectively $1rad$ for rotational modes. The Aerodynamic Influence Coefficient matrix $\mathbf{A}_{IC}$ is computed by the subsonic panel method ZONA6, within the Aeroelastic Toolkit ZAERO (Version (2009)). Matrix $\mathbf{A}_{IC}$ relates normal wash ($\mathbf{w}$) to unsteady pressure coefficients ($\mathbf{C_p}$) on aerodynamic panels, which are normalized by dynamic pressure. Matrices $\mathbf{A}_{IC}(ik)$ are computed in frequency domain for a set of reduced frequencies (k).

$$\mathbf{C_p} = [\mathbf{A}_{IC}(ik)]^T \mathbf{w}, \tag{7}$$

here,

$$k = \frac{\omega c}{2V_\infty}, \tag{8}$$

Thereby, ω is the angular frequency, c is the reference chord length and V_∞ denotes the free stream velocity. By the use of an integration matrix $\mathbf{S}_{KJ}$, $\mathbf{C_p}$ is converted to aerodynamic force coefficients in the 6-DOF directions of each panel. For the transformation of 6-DOF displacements on panels to normal wash the transformation matrix $\mathbf{F}_{JKS}$ is employed. As

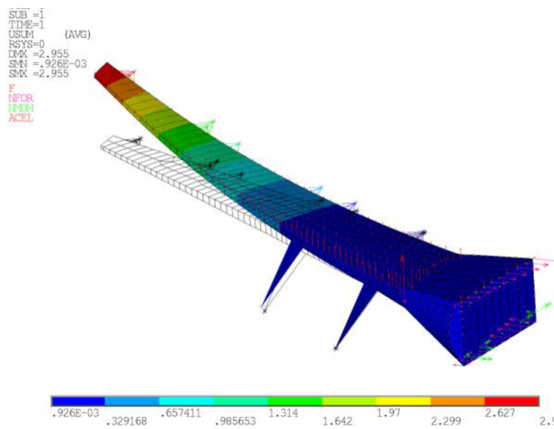

Figure 4: Deformation of the wing due to gravitational and aerodynamic forces at 1g-level flight, Ma = 0.85, q = 11069Pa Kozek and Schirrer (2015); Wildschek et al. (2010).

panel control points do not coincide with structural grid points, a spline matrix $\mathbf{G}$ is used which transforms displacements or forces from structural to aerodynamic DOF. Finally, the modal matrix $\mathbf{\Phi}$, on structural DOF, transforms the aerodynamic force coefficients to modal coordinates resulting in the Generalized Aerodynamic Forces (GAF) due to modal deflection $\mathbf{Q}_{hh}$. GAF due to control surface deflection$\mathbf{Q}_{hc}$ and due to gust downwash $\mathbf{Q}_{hg}$ are computed by right-hand side multiplication with control surface modes $\mathbf{Q}_c$ and gust modes $\mathbf{Q}_g$ (Version (2009)), see Eq. 9.

$$
\begin{aligned}
\mathbf{Q}_{hh}(ik) &= \mathbf{\Phi}^T\mathbf{G}^T[\mathbf{S}_{KJ}]^T[\mathbf{A}_{IC}(ik)]^T[\mathbf{F}_{JKS}(ik)]^T\mathbf{G}\mathbf{\Phi}\\
\mathbf{Q}_{hc}(ik) &= \mathbf{\Phi}^T\mathbf{G}^T[\mathbf{S}_{KJ}]^T[\mathbf{A}_{IC}(ik)]^T[\mathbf{F}_{JKS}(ik)]^T\mathbf{G}\mathbf{\Phi}_c\\
\mathbf{Q}_{hg}(ik) &= \mathbf{\Phi}^T\mathbf{G}^T[\mathbf{S}_{KJ}]^T[\mathbf{A}_{IC}(ik)]^T[\mathbf{F}_{JKS}(ik)]^T\mathbf{G}\mathbf{\Phi}_g
\end{aligned}
\tag{9}
$$

In order to derive equations of motion in time-domain, the GAF are approximated in Laplace-domain by the Minimum-State Method (Karpel (1982)). By replacing iw with the Laplace variable s the approximation formula in Laplace domain gets:

$$
\begin{aligned}
\mathbf{Q}_{hh}(s) = \mathbf{A}_{hh0} + \frac{c}{2V_\infty}\mathbf{A}_{hh1}s + \left(\frac{c}{2V_\infty}\right)^2\mathbf{A}_{hh1}s^2 + \mathbf{D}\left(\mathbf{I}s - \frac{2V_\infty}{c}\mathbf{R}\right)^{-1}\mathbf{E}_h s \\
\mathbf{Q}_{hc}(s) = \mathbf{A}_{hc0} + \frac{c}{2V_\infty}\mathbf{A}_{hc1}s + \mathbf{D}\left(\mathbf{I}s - \frac{2V_\infty}{c}\mathbf{R}\right)^{-1}\mathbf{E}_c s \\
\mathbf{Q}_{hg}(s) = \mathbf{A}_{hg0} + \frac{c}{2V_\infty}\mathbf{A}_{hg1}s + \mathbf{D}\left(\mathbf{I}s - \frac{2V_\infty}{c}\mathbf{R}\right)^{-1}\mathbf{E}_g s
\end{aligned}
\tag{10}
$$

The system matrices of the aeroelastic equations of motion, $\mathbf{K}$, $\mathbf{B}$, and $\mathbf{M}$ are composed of approximation matrices of aerodynamic forces and structural portions, i.e. modal stiffness $\mathbf{K}_{struct}$, modal damping $\mathbf{B}_{struct}$ and modal mass $\mathbf{M}_{struct}$ (Version (2009)).

$$
\begin{aligned}
\mathbf{K} &= \mathbf{K}_{struct} + q_\infty \mathbf{A}_{hh0} \\
\mathbf{B} &= \mathbf{B}_{struct} + q_\infty\left(\frac{c}{2V_\infty}\right)\mathbf{A}_{hh1} \\
\mathbf{M} &= \mathbf{M}_{struct} + q_\infty\left(\frac{c}{2V_\infty}\right)\mathbf{A}_{hh2}
\end{aligned}
\tag{11}
$$

3.3. Coupled Equations of Motion

The aspired inputs to the coupled flight dynamic-aeroelastic model are control surface deflections, gust inputs, and engine thrust. The outputs are accelerations, rates and angular displacements at the CG, vertical accelerations of the wing tips, angle of attack and sideslip angle, as well as cut forces and moments at the wing roots and vertical stabilizer roots. The aeroelastic input equation for rigid and elastic motion in state-space form (Version (2009)) is given as:

$$
\dot{x} = \begin{Bmatrix} \dot{q} \\ \ddot{q} \\ \dot{x_a} \end{Bmatrix} = A_{ss}x + B_{ss}u = \begin{bmatrix} 0 & 1 & 0 \\ -M^{-1}K & -M^{-1}B & -q_\infty M^{-1}D \\ 0 & E_h & \frac{V}{L}R \end{bmatrix} \begin{Bmatrix} q \\ \dot{q} \\ x_a \end{Bmatrix} +
$$
$$
\begin{bmatrix} 0 & 0 & 0 & 0 \\ -q_\infty M^{-1}A_{hC_0} & -\frac{q_\infty L}{V}M^{-1}A_{hC_1} & -\frac{q_\infty}{V}M^{-1}A_{hG_0} & -\frac{q_\infty L}{V^2}M^{-1}A_{hG_1} \\ 0 & E_C & 0 & \frac{1}{V}E_G \end{bmatrix} \begin{Bmatrix} \delta \\ \dot{\delta} \\ \eta \\ \dot{\eta} \end{Bmatrix}
\tag{12}
$$

Thereby, $\mathbf{q}$, $\mathbf{x_a}$, δ , and η denote vectors of modal deflections, aerodynamic lag states, control surface deflections, and gust velocities. In order to account for realistic flight dynamics, the steady aerodynamic data (see Section 3.2) for the rigid aircraft is used to build up linear 6-DOF flight-dynamics equations of motion (Baldelli et al. (2006)). By similarity transformation the rigid body states, namely translations T_x, T_y, T_z and rotations R_x, R_y, R_z and their time derivatives are transformed to flight-dynamic states:

$$X_{F,lon} = \begin{bmatrix} x \\ u \\ h \\ w \\ \theta \\ q \end{bmatrix} = \begin{bmatrix} -1 & 0 & 0 & 0 & 0 & 0 \\ 0 & 0 & 0 & -1 & 0 & 0 \\ 0 & 1 & 0 & 0 & 0 & 0 \\ 0 & 0 & V_\infty & 0 & -1 & 0 \\ 0 & 0 & 1 & 0 & 0 & 0 \\ 0 & 0 & 0 & 0 & 0 & 1 \end{bmatrix} \begin{bmatrix} T_x \\ T_z \\ R_y \\ \dot{T}_x \\ \dot{T}_z \\ \dot{R}_y \end{bmatrix} \tag{13}$$

$$X_{F,lat} = \begin{bmatrix} y \\ \beta \\ p \\ r \\ \phi \\ \psi \end{bmatrix} = \begin{bmatrix} 1 & 0 & 0 & 0 & 0 & 0 \\ 0 & 0 & 1 & \frac{1}{V_\infty} & 0 & 0 \\ 0 & 0 & 0 & 0 & -1 & 0 \\ 0 & 0 & 0 & 0 & 0 & -1 \\ 0 & -1 & 0 & 0 & 0 & 0 \\ 0 & 0 & -1 & 0 & 0 & 0 \end{bmatrix} \begin{bmatrix} T_y \\ R_x \\ R_z \\ \dot{T}_y \\ \dot{R}_x \\ \dot{R}_z \end{bmatrix} \tag{14}$$

The resulting state vector $\mathbf{x}$, contains the 12 airframe states, followed by elastic mode states ξ , their first time derivatives $\ddot{\xi}$ and lag states $\mathbf{x_a}$, see Eq. (15).

$$\mathbf{x} = \begin{bmatrix} \mathbf{x}_{F,lon} & \mathbf{x}_{F,lat} & \xi & \ddot{\xi} & \mathbf{x_a} \end{bmatrix} \tag{15}$$

The flight dynamic portion of the equations of motion, i.e. the 12×12 sub-matrix of the matrix $\mathbf{A_{ss}}$ related to the airframe states, has to represent the true flight dynamic behaviour of the aircraft and can now be replaced by linear flight-dynamics, derived from steady aerodynamics. The measurement equations are given as:

$$\begin{Bmatrix} y_F \\ y_{struct} \\ \dot{y}_{struct} \\ \ddot{y}_{struct} \\ \dot{y}_{moment} \end{Bmatrix} = \begin{bmatrix} C_F \\ C_{def} \\ C_{vel} \\ C_{vel} A_{ss} \\ C_{moment} \end{bmatrix} x + \begin{bmatrix} 0 \\ 0 \\ 0 \\ C_{vel} B_{ss} \\ 0 \end{bmatrix} \begin{Bmatrix} \delta \\ \dot{\delta} \\ \eta \\ \dot{\eta} \end{Bmatrix} s \tag{16}$$

Where $\mathbf{C}_F$, $\mathbf{C}_{def}$, $\mathbf{C}_F$, and $\mathbf{C}_{moment}$ are the output matrices for flight-dynamics $\mathbf{y}_F$, structural deformations $\mathbf{y}_{struct}$, structural velocities struct $\dot{\mathbf{y}}_{struct}$, and wing root bending moment measurement $\mathbf{y}_{moment}$. Structural acceleration outputs $\ddot{\mathbf{y}}_{struct}$ are facilitated by the time-derivative of the structural velocity output equation and replacing $\dot{\mathbf{x}}$ by the right-hand side of the input Eq. (12).

The wing is one of the most important components to evaluate lift, drag, and moment characteristics. The forces and moments on the aerofoil is calculated by cutting the aerofoil into sections for which the pressure distribution (c_p) is solved either by mathematical functions based on the geometry or by existing computation programs requiring only the most crucial parameters as input. This enables the deduction of 2D forces and moments of the aerofoil and is then integrated over the y-axis (lateral direction) over the entire span for a 3D solution.

3.4. Model Order Reduction

This section describes the generation of a parameterized state space model of the coupled flight dynamic-aeroelastic equations of motion of the NACRE-BWB aircraft. The order of this model is subsequently reduced for control law design and validation by a combination of objective methods (balanced reduction) and prior choice of preserved states (i.e. all flight mechanics states and lag states). The model before reduction had 210 states including 10 lag states, 12 flight mechanic states and 188 states corresponding to elastic modes. The first attempt of the generation of the reduced order model (ROM) has been the balanced reduction based on the given inputs and outputs with target model dimension (e.g. 14 states, 50 states etc.). The result illustrated in Fig. 5 show that such reduction can discard some important states, like first bending modes, lag states, or even flight mechanic states (Wildschek et al. (2010)).

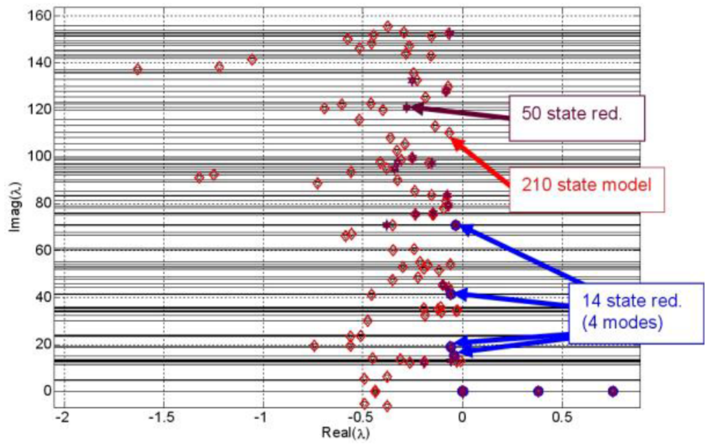

Figure 5: Eigen values for different number of states kept in the model using balanced reduction (Kozek and Schirrer (2015); Wildschek et al. (2010)).

The red poles correspond to the initial 210 state model, magenta poles to the 50 states ROM and blue poles to the 14 states ROM. Therefore, the direct usage of the balanced reduction for all outputs and all inputs cannot be considered ideal. Thus, a modified approach is applied. All original 10 lag states as well as the 12 flight mechanic states are preserved. The order reduction was subsequently adapted based on the comparison of singular value characteristics and transfer functions for different levels of reduction. The validation model contains 12 aeroelastic modes (i.e. modes number 1-5, 11-14, 17, 21, and 23) which were chosen using Singular Perturbation Approximation (SPA) variant of balanced reduction (Wildschek et al. (2010)). The final model for control law synthesis additionally contains the first 4 (corresponding to 4 lowest Eigen frequencies) aeroelastic modes. The reduced order model is validated on the purely nonlinear model at a wide range of frequencies details can be found in Kozek and Schirrer (2015).

4. Control Law Design

4.1. $\eta_{\mathbf{z}}$ Law

The wing root loading of a flexible aircraft is evaluated by estimating the vertical acceleration at various locations in the aircraft. In principle, for precise determination of the wing root loading on the aircraft, the acceleration must be estimated at the the centre of gravity (CG), left and right wing-tip node ((Alam et al., 2015)). A related detailed description on the optimal positioning for acceleration estimation in order to determine wing loading are outlined in (Haniš and Hromčík (2011); Kammer (1996)). The relative acceleration between the wing-tips and CG is defined as η_z law. η_z law gives an indirect measure of wing root loading experienced by the aircraft. The relation between the control input and η_z law is used to design the load alleviation controllers. The η_z law is calculated by:

$$\eta_{z_{law}} = \overbrace{\frac{1}{2}\eta_{z_{wingtip}}}^{leftnode} + \overbrace{\frac{1}{2}\eta_{z_{wingtip}}}^{rightnode} - \eta_{z_{CG}} \tag{17}$$

4.2. Signal Shaper Design

Fig. 6a shows the main control surfaces of the NACRE-BWB aircraft. Structural loads and vibration of BWB aircraft caused by the pilot's commands (in the presented case, push-pull action of the elevator) can be significantly reduced by active damping. The aim of this control design is to design a feedforward signal shaping (DZV) controller which will attenuate the vibration effect reducing the wing root moments and forces of the aircraft as shown in the control block scheme in Fig. 6b.

In real flights wing root forces and moments can not be measured. However an indirect measure of wing root moments and forces are given by the η_z law as described in Section 4.1. Therefore the aim of the DZV controller is to damp the flexible modes connecting the Elevator channel to η_z law. A two-stage control law is designed; an independent stability augmented system (SAS) or control augmented system (CAS) and the feedforward DZV controller, as shown in Fig 6b. The SAS or CAS primarily take care of the rigid body longitudinal flight dynamics damping the pitch rate. And the feedforward DZV controller damps the vibrations associated with the flexible modes. Such control structure have clear advantages. First with respect to the tuning of the controllers (both the controllers SAS or CAS and DZV can be designed/tuned independently). Second, during the flight testing the newly proposed DZV controller can be turned on/off while ensuring the full control of the aircraft. Thirdly, from the important flight safety point of view, the loss of such an add-on DZV controller is not a critical failure and will not take the aircraft out of control. When both the switches in the block

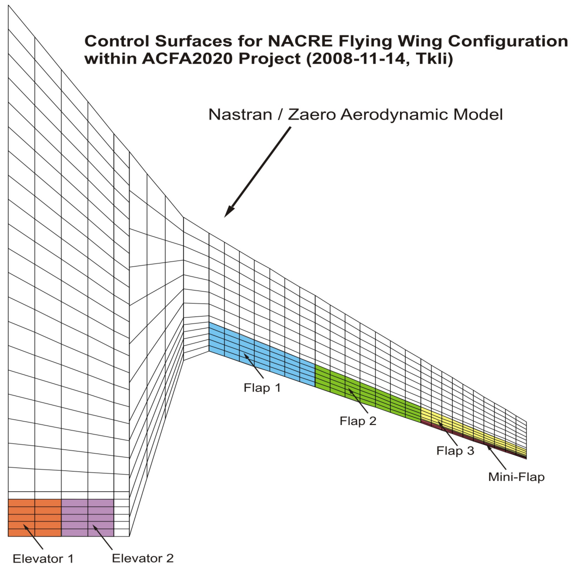

(a) Control surfaces of NACRE aircraft.

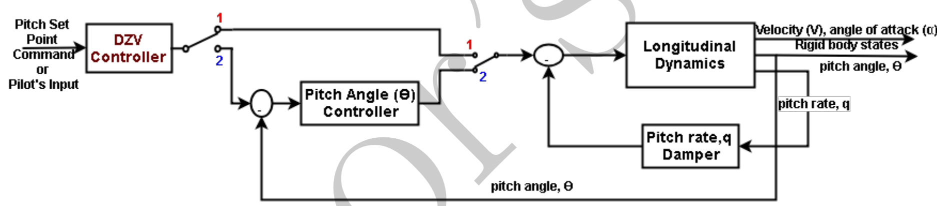

(b) Control block scheme for the input shaper.

Figure 6: NACRE aircraft primary control surfaces and the proposed control block scheme.

diagram in Fig 6b are in position 1, the DZV controller is engaged with SAS. When both the switches are in position 2, the DZV controller is engaged with CAS. For the demonstration of the advantages of DZV controllers a simple of loop by loop SAS and CAS design considered in this article[2]. More advanced SAS and CAS design using multivariable feedback techniques can be found at Goupil (2011).

Fig 7 show the frequency responses of the original aircraft from Elevator to η_z law. It can be seen that there are two peaks in the frequency response

[2]Please note the focus of this paper is to design feedforward controller not to design multivaraible stabilising SAS or CAS

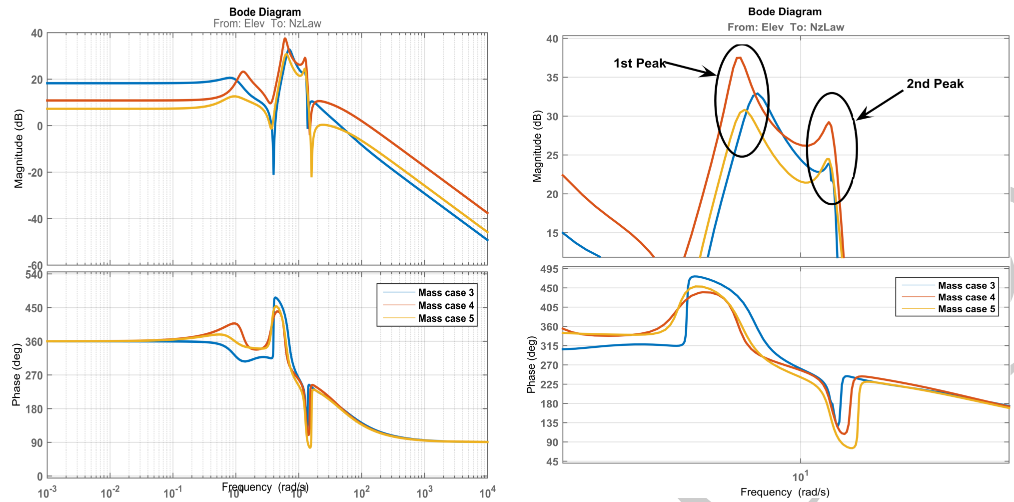

(a) Frequency response of the original aircraft.

(b) Zoomed frequency response of the original aircraft.

Figure 7: Frequency response from the elevator channel to η_z law of the original aircraft at various mass cases.

one at approximately at 5.94 rad/s and 12.58 rad/s. These two peaks at the particular frequency are accounted for the flexible vibrations of the aircraft.

Described in the Section 2 that only one frequency can be damped by one DZV controller. Therefore for the design case, Mass case 4 was chosen due to the fact it having the lowest frequency. Following (2), the parameters calculated for the DZV controller are $\omega_n = 5.94 rad/s$, $\zeta = 0.1$,$\alpha = 0.25$, $A = 0.4254$ and $T = 0.4020$. The complete transfer function of the DZV controller is given by:

$$DZV(s) = 0.4254 + 1.9058 \left(\frac{e^{-0.1005s - e^{-0.4020s}}}{s} \right). \tag{18}$$

For the comparison a traditional Butterworth and Bessel structural filter has been designed following the Eq. (19) and (21) (Elliott (1987)):

$$Butterworth\ (s) = \frac{\omega_p^2}{s^2 + \sqrt{2}\omega_p s + \omega_p^2} \tag{19}$$

$$Butterworth\ (s) = \frac{35.28}{s^2 + 8.4s + 35.28} \tag{20}$$

$$Bessel\ (s) = \frac{\theta_n(0)}{\theta_n(s/\omega_p)} \tag{21}$$

$$Bessel\ (s) = \frac{35.28}{s^2 + 10.8s + 35.28} \tag{22}$$

Here ω_p is the chosen cut-off frequency. $\theta_n(s)$ is the reverse Bessel polynomial form which the filter gets its name. The cut-off frequency is chosen to be $5.94 rad/s$. Additionally a modified notch filter is designed to compare the performance of the DZV controller. The general equation for notch filter is given by Eq. (23). Due to the general notch filter having the same order in the denominator and numerator of the transfer function, it gives a high feed-forward control input which often leads to control input saturation in applications like flight control. Hence the general notch filter is modified with a simple 1st order low-pass roll-off filter at the cut-off frequency as shown in Eq. (24).

$$General\ Notch\ (s) = \frac{s^2 + \omega_p^2}{s^2 + Q\omega_p s + \omega_p^2} \tag{23}$$

Here Q is the fading factor.

$$Notch\ (s) = \overbrace{\frac{s^2 + \omega_p^2}{s^2 + Q\omega_p s + \omega_p^2}}^{General\ Notch} \overbrace{(\frac{\omega_p}{s + \omega_p})}^{Low-pass\ Filter} \tag{24}$$

$$Notch\ (s) = \frac{5.94s^2 + 2.97s + 209.6}{s^3 + 7.94s^2 + 47.16s + 35.28} \tag{25}$$

Fig. 8 shows the comparison of controllers in time domain and in frequency domain. Fig. 9 shows the frequency response of the damped aircraft with respect to the original aircraft for aircraft mass case 4.

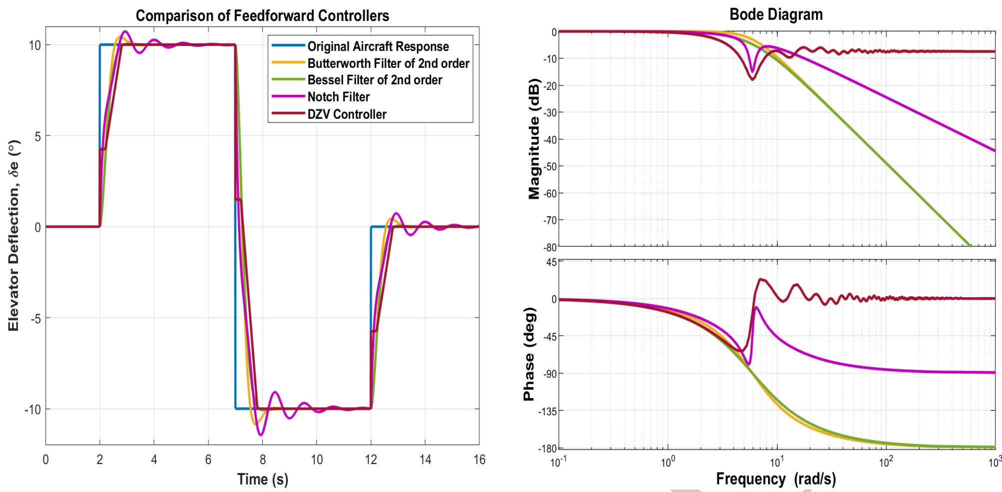

(a) Controller's response to push-pull manoeuvre.

(b) Controller's frequency response.

Figure 8: Comparison of various controllers.

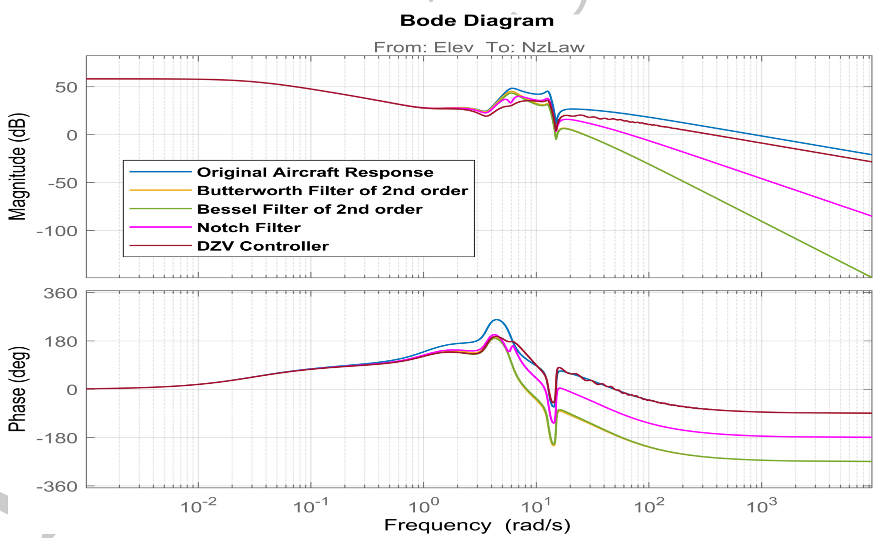

Figure 9: Frequency response of original aircraft and damped aircraft with various feed-forward controller engaged for Mass Case 4.

It can be seen from Fig. 9 that the 1st peak is approximately damped by 5dB and the 2nd peak is approximately damped by 3dB. This reduction of the peak in the Elevator to η_z law reduces the over all wing root forces and moments. A critical design requirement for the DZV controller is not to excite the low frequency of the aircraft. From the Fig. 9 it can be seen that the low frequency of the aircraft is not excited and the high frequency is further attenuated. Complete simulation results are discussed in the next section.

5. Simulation Results and Discussion

Seven different mass cases are considered for the simulations. For a realistic simulation, the rate limiters and the saturation of the elevator (actuators) were taken into consideration. Elevators are saturated at $\pm 30^o$ with a rate limited by $\pm 30^o/s$. A push-pull elevator deflection was given through the elevator channel as an exogenous signal (as shown in Fig. 8) for artificially exciting the flexible modes of the aircraft. M_x is defined as the wing root bending moments, M_y is defined as the wing root torsional moments and M_z is defined as the moments along the $Z - axis$ of the aircraft. F_x is defined as the shear force along $X - axis$ of the aircraft, F_y is defined as the shear force along $Y - axis$ of the aircraft and F_z is defined as the shear force along $Z - axis$ of the aircraft. Fig. 11 to Fig. 12 show the aircraft responses at mass case 1, 4 and 7 respectively (responses to other mass cases 2,3 and 5 were similar). For the analysis, every plots represent responses to five different instances. The blue line indicates the response of the original SAS aircraft only; the yellow, green and magenta line indicates the aircraft's response with the traditional Butterworth, Bessel and notch filter engaged; finally the red line indicates the aircraft's response with newly proposed DZV feedforward controller engaged. Simulations were carried out using MATLAB/Simulink. The response of the rigid body states of the aircraft such as pitch rate and pitch angle were stable (as shown in Fig. A.14 for mass case 4). The wing root moments and force values are normalized with respect to the maximum value occurring to the original aircraft's response[3].

[3] Due to industry related confidential reasons the exact values of the wing root moments and forces cannot be published, however for the better judgement of the reviewers, the dimensional plots for Fig. 11 to Fig. 12 are provided as an addition material.

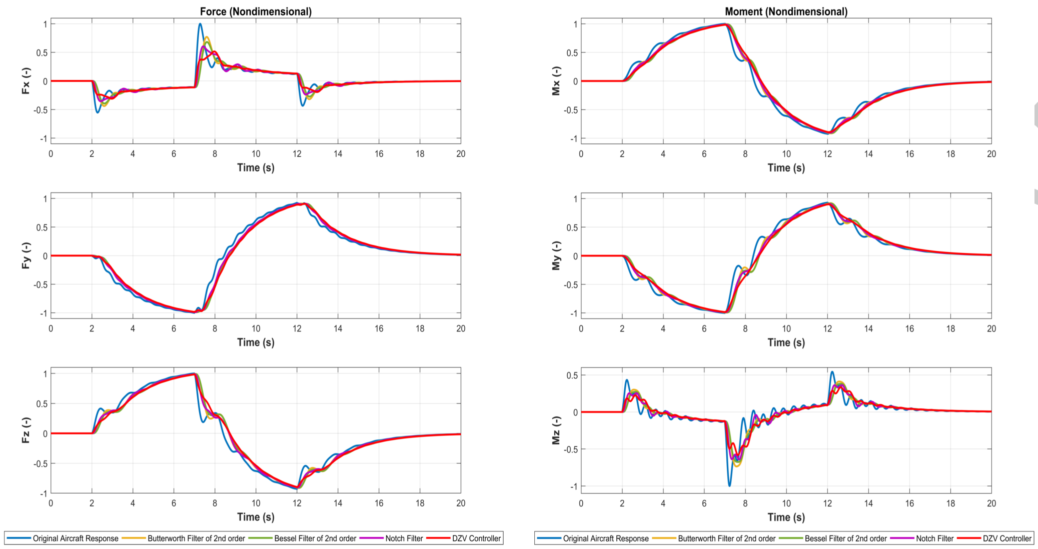

(a) Wing root forces. (b) Wing root moments.

Figure 10: Normalized wing root forces (F_x, F_y, F_z) and moments (M_x, M_y, M_z) for Mass Case 1.

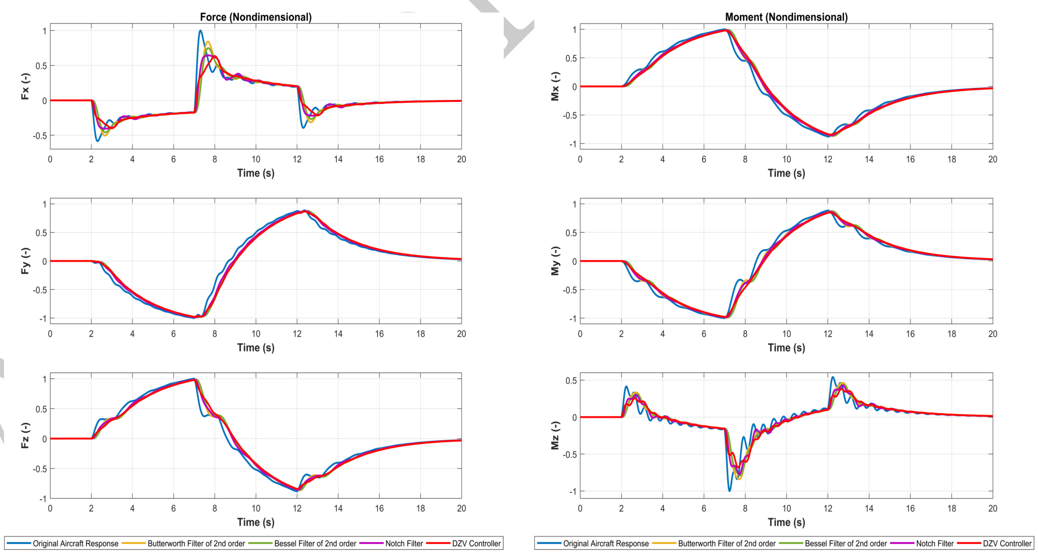

(a) Wing root forces. (b) Wing root moments.

Figure 11: Normalized wing root forces (F_x, F_y, F_z) and moments (M_x, M_y, M_z) for Mass Case 4.

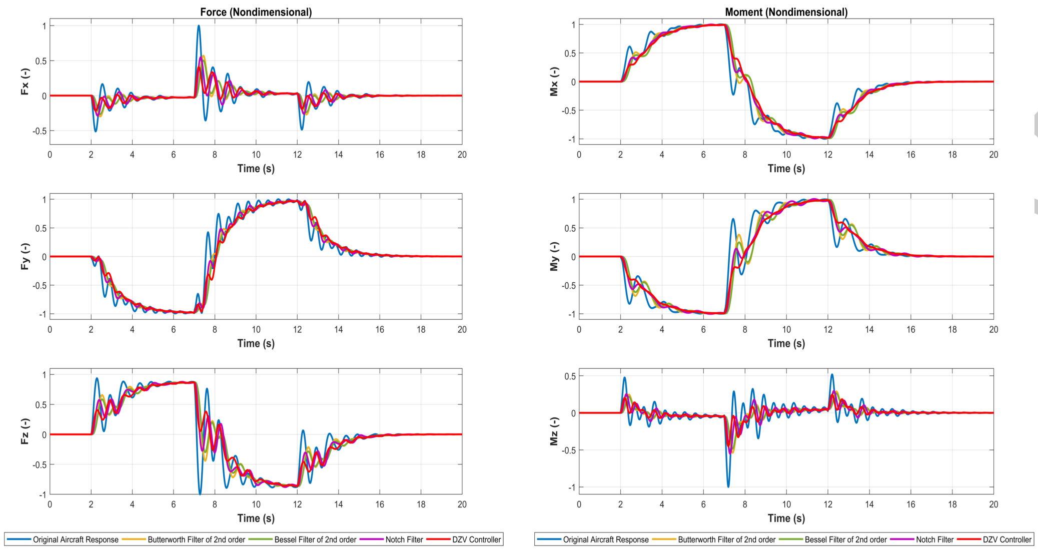

(a) Wing root forces.

(b) Wing root moments.

Figure 12: Normalized wing root forces (F_x, F_y, F_z) and moments (M_x, M_y, M_z) for Mass Case 7.

Observing Fig. 11 to Fig. 12, it can be seen that all the controllers (Butterworth, Bessel, notch and DZV) are reducing the wing root loading compared to the original aircraft response with only SAS. However it can be seen that the DZV controller and notch filter are performing significantly well in reducing the peak value of the wing root forces and moments compared to the traditional low pass filters like Butterworth and Bessel for designed Mass Case 4. The overall values of the reduction in the peak values for all the mass cases are summarized in the Table A.2 in Appendix A. The reduction in the peak is calculated as:

$$\% = \frac{peak\ original\ aircraft - peak\ aircraft\ using\ FF\ controller}{peak\ original\ aircraft} \times 100 \quad (26)$$

From the Table A.2 in Appendix A it can be noticed the performance of the notch filters deteriorates over Mass Cases 5,6 and 7. It is due to the fact that notch filters are sensitive to modelling frequency compared to the DVZ filter. DZV filter are comparatively insensitive to modelling due to its retarded spectral features. For details more details on this reader can see Vyhlídal and Hromčík (2015). It can also be seen that the oscillatory effect on the forces and moments are reduced while using the traditional low pass filter and the newly proposed DZV controller compared to the original aircraft's response. To quantify the result of this improvement in the reduction of oscillatory motion, first we take the derivative of the respective forces and moments, followed by taking the absolute value of the derivative, then calculate the area under the curve over the whole simulation time. This way we can calculate the total wing loading experienced at the wing root due to the oscillatory nature of the loading. Fig. 13 illustrates the complete process for mass case 4 considering the F_x.

As illustrated in Fig. 13, in such a way we can calculate the total force and moments absorbed by the wing root over the simulation time. Mathematically it is presented as:

$$Total\ force\ or\ total\ moment = \int_0^T \mid \frac{derivative\ of\ force\ or\ moment}{dt} \mid dt. \quad (27)$$

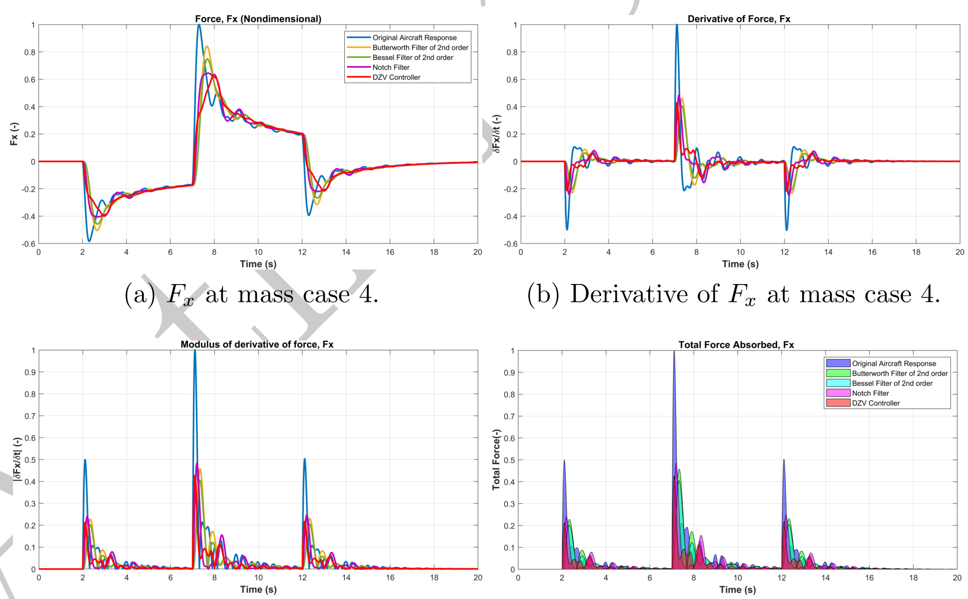

(a) F_x at mass case 4.

(b) Derivative of F_x at mass case 4.

(c) Modulus of the derivative of F_x.

(d) Integral (area under the curve) of the modulus of the derivative of F_x.

Figure 13: Illustration of calculation for performance improvement in reducing oscillatory wing loading.

Following Eq. (27) total forces and moments experienced at the wing root due to the oscillatory wing loading for each axis is calculated. The percentage improvement in the total force and moments is calculated as below, and summarized in Table A.3, in Appendix A:

$$\% = \frac{total\ area\ of\ original\ aircraft - total\ area\ using\ FF}{total\ area\ of\ original\ aircraft} \times 100$$

From the Table A.3, it can be seen that the proposed DZV controller performs significantly well compared to the Butterworth, Bessel or notch filter in terms of reducing the oscillatory wing root loading. This oscillatory wing loading is directly related to the fatigue of the airframe. The reduction in the oscillatory behaviour of forces and moments at the wing root extends the structural lifetime of the airframe.

Of course the DZV controller is slightly slower than the traditional low pass filters, however the response time for the DZV controller is of the same order as traditional low pass filter, Butterworth, Bessel as shown in Fig. 8. The response of the rigid body states of the aircraft such as pitch rate and pitch angle are comparable (as shown in Fig. A.14 for mass case 4). Given the newly proposed DZV controller is providing significantly improved performance, the trade-off between the response time and the improvement in the performance in load alleviation is always beneficial. The simulation results from Fig. 11 to Fig. 12 show that significant performance improvement is achievable in terms of reduction in the peak values of the wing root forces and moments by using DZV controller as an alternative to traditional low-pass filters. On an average by using the DZV controller the performance was improved by 17.4% and 18.9% with respect to reduction in the maximum peak values in forces and moments at the wing root. In addition by using the DZV controller the average reduction in the oscillatory effect of wing root forces and moments was improved by 34.88% and 36.64% respectively.

The peaks in the wing root forces and moments indicates the maximum load experienced by the aircraft at the wing root. These peak values of wing loads provide the requirement for the reinforcement needed at the wing root joints, hence works as a sizing condition for the wing root joints. Therefore, due to the achievable peaks reduction by the proposed DZV controller, it indicates a prospective option for structural weight savings, in other words cost reduction and economic benefits. In addition to that, by reducing the oscillatory effects on wing root loading, the signal shaping DZV controller provides a possible option for reducing structural failures such as fatigues, in other words extending the lifetime of the airframe.

6. Conclusions

According to the presented simulation case study, application of signal shapers instead of the structural low-pass filters can be highly recommended for flexible aircraft. The proposed DZV controller provides significantly improved performance with respect to the reduction of peak values and oscillatory nature of the induced wing root loading (forces and moments) depending on the various mass cases as compared to the traditional structural Butterworth, Bessel or notch filters if similar signal lags are allowed. Robustness of the proposed solution with respect to flight envelope and aircraft configuration changes appears acceptable in spite of the fact that the proposed control solution uses no feedback. It is partly due to the fact that the sensitivity of the DZV shaper at higher-frequencies is slightly better in comparison to related classical lumped-delay shapers as reported by Vyhlídal et al. (2013a) and Vyhlídal and Hromčík (2015).

Acknowledgments

The research of M. Alam was supported by the Czech Technical University in Prague under internal grant no. SGS17/137/OHK3/2T/13. The research of M. Hromcik was supported by the Czech Science Foundation (GACR) under grant no. 19-16772S. The authors would like to thank Airbus Group Innovations (formerly know as EADS Innovation Works, Munich) and all the related partners in the ACFA 2020 consortium (www.acfa2020.eu) for sharing the aircraft's dynamic model.

References

ACFA, C. (2008). Commissione europea : CORDIS : Progetti e risultati : Active Control for Flexible 2020 Aircraft.

Alam, M. (2014). Combined feedforward/feedback gust load alleviation control for highly flexible aircraft. In *Proceedings of 2014 PEGASUS-AIAA Student Conference*, pages 1–12.

Alam, M., Hromcik, M., and Hanis, T. (2015). Active gust load alleviation system for flexible aircraft: Mixed feedforward/feedback approach. *Aerospace Science and Technology*, 41(1):122–133.

Alikoç, B., Vyhlídal, T., and Ergenç, A. F. (2016). Closed-form smoothers and shapers with distributed delay for damped oscillatory modes. *IET Control Theory & Applications*, 10(18):2534–2542.

Baldelli, D. H., Chen, P. C., and Panza, J. (2006). Unified Aeroelastic and Flight Dynamic Formulation via Rational Function Approximations. *Journal of Aircraft*, 43(3):763–772.

Burlion, L., Poussot-Vassal, C., Vuillemin, P., Leitner, M., and Kier, T. (2014). Longitudinal manoeuvre load control of a flexible large-scale aircraft. *IFAC Proceedings Volumes*, 47(3):3413–3418.

Cambier, L. and Kroll, N. (2008). MIRACLE - a joint DLR/ONERA effort on harmonization and development of industrial and research aerodynamic computational environment. *Aerospace Science and Technology*, 12(7):555–566.

Cole, M. O., Shinonawanik, P., and Wongratanaphisan, T. (2018). Time-domain prefilter design for enhanced tracking and vibration suppression in machine motion control. *Mechanical Systems and Signal Processing*, 104:106–119.

Elliott, D. F. (1987). *Handbook of Digital Signal Processing: Engineering Applications*. Academic Press.

Frota, J. (2010). NACRE novel aircraft concepts. *Aeronautical Journal*, 114(1156):399–404.

Goupil, P. (2011). Airbus state of the art and practices on fdi and ftc in flight control system. *Control Engineering Practice*, 19(6):524–539.

Haniš, T. and Hromčík, M. (2011). Information-based sensor placement optimization for BWB aircraft. In *IFAC Proceedings Volumes (IFAC-PapersOnline)*, volume 18, pages 2236–2241.

Hepperle, M. (2005). The VELA Project. *Assessment*, 2002(October 2002):4.

Hoogendijk, R., Heertjes, M., Van de Molengraft, M., and Steinbuch, M. (2014). Directional notch filters for motion control of flexible structures. *Mechatronics*, 24(6):632–639.

Hromčík, M. and Vyhlídal, T. (2017). Inverse feedback shapers for coupled multibody systems. *IEEE Transactions on Automatic Control*, 62(9):4804–4810.

Kammer, D. C. (1996). Optimal sensor placement for modal identification using system-realization methods. *Journal of Guidance, Control, and Dynamics*, 19(3):729–731.

Karpel, M. (1982). Design for Active Flutter Suppression and Gust Alleviation Using State-Space Aeroelastic Modeling. *Journal of Aircraft*, 19(3):221–227.

Kozek, M. and Schirrer, A. (2015). *Modeling and Control for a Blended Wing Body Aircraft*. Advances in Industrial Control. Springer International Publishing, Cham.

M. Smith, O. (1957). Posicast Control of Damped Oscillatory Systems. *Proceedings of the IRE*, 45(9):1249–1255.

McLean, D. (1990). *Automatic flight control systems*. Prentice Hall.

Miller, C. (2011). Nonlinear dynamic inversion baseline control law: architecture and performance predictions. In *AIAA Guidance, Navigation, and Control Conference*, page 6467.

Oh, C.-S., Bang, H., and Park, C.-S. (2008). Attitude control of a flexible launch vehicle using an adaptive notch filter: ground experiment. *Control Engineering Practice*, 16(1):30–42.

Pilbauer, D., Michiels, W., and Vyhlídal, T. (2016). A comparison of shaper-based and shaper-free architectures for feedforward compensation of flexible modes.

Pratt, R. W., Taylor, R., and Caldwell, B. D. (1994). Aeroservoelasticity: Key Issues Affecting the Design of Flight Control Systems. In *International Conference on Control*, volume 2, pages 1522–1527. IEE.

R. Taylor, R. Pratt, B. C. (1996). Alternative approach to aeroservoelastic design and clearance. *IEE Proceedings - Control Theory and Applications*, 143(1):1–8.

Singer, N. C. and Seering, W. P. (1990). Preshaping Command Inputs to Reduce System Vibration. *Journal of Dynamic Systems, Measurement, and Control*, 112(1):76.

Singhose, W., Derezinski, S., and Singer, N. (1996). Extra-insensitive Input Shapers for Controlling Flexible Spacecraft. *Journal of Guidance, Control, and Dynamics*, 19(2):385–391.

Singhose, W., Eloundou, R., and Lawrence, J. (2010). Command generation for flexible systems by input shaping and command smoothing. *Journal of guidance, control, and dynamics*, 33(6):1697–1707.

Singhose, W., Seering, W., and Singer, N. (1994). Residual Vibration Reduction Using Vector Diagrams to Generate Shaped Inputs. *Journal of Mechanical Design*, 116(2):654.

Stevens, B. L., Lewis, F. L., and Johnson, E. N. (2015). *Aircraft Control and Simulation: Dynamics, Controls Design, and Autonomous Systems*. Wiley.

Su, W. and S. Cesnik, C. E. (2010). Nonlinear Aeroelasticity of a Very Flexible Blended-Wing-Body Aircraft. *Journal of Aircraft*, 47(5):1539–1553.

Torralba, J., Puyou, G., and Demourant, F. (2009). Self-scheduling multiobjective control law design for a flexible aircraft. In *AIAA Guidance, Navigation, and Control Conference*, page 6303.

Tuzcu, I. (1999). *Dynamics and Control of Flexible Aircraft*. PhD thesis, Virginia Tech.

Version, Z. (2009). 8.4 user's manual engineers' toolkit for aeroelastic solutions, zona technology. *Inc., Scottsdale, AZ*.

Vyhlídal, T. and Hromčík, M. (2015). Parameterization of input shapers with delays of various distribution. *Automatica*, 59:256–263.

Vyhlídal, T., Hromčík, M., Kučera, V., and Anderle, M. (2016). On Feedback Architectures with Zero-Vibration Signal Shapers. *IEEE Transactions on Automatic Control*, 61(8):2049–2064.

Vyhlídal, T., Kučera, V., and Hromčík, M. (2013a). Signal shaper with a distributed delay: Spectral analysis and design. *Automatica*, 49(11):3484–3489.

Vyhlídal, T., Kučera, V., and Hromčík, M. (2013b). Zero vibration shapers with distributed delays of various types. In *Proceedings of the IEEE Conference on Decision and Control*, pages 940–945. IEEE.

Wildschek, A., Stroscher, F., Klimmek, T., Šika, Z., Vampola, T., Valášek, M., Gangsaas, D., Aversa, N., and Berard, A. (2010). Gust load alleviation on a large blended wing body airliner. In *27th international congress of the aeronautical sciences, Nice, France*.

Appendix A. Appendix A

Summarized reduction in the peak and the total absorbed of the wing root forces and moments in Table A.2 and A.3.

Fig. A.14 show the aircraft's rigid body state's response for mass case 4. Responses to all other mass cases are similar.

	% Improvements							
Mass Case	**1**	**2**	**3**	**4**	**5**	**6**	**7**	**Average**
F_x- **DZV**	48.40	2.46	41.84	36.54	61.47	58.91	58.92	44.08
F_x- **Butterworth**	22.86	1.78	18.98	15.83	26.76	42.55	42.98	24.54
F_x- **Bessel**	31.85	2.23	28.15	25.15	35.37	49.31	49.67	31.67
F_x- **Notch**	39.92	1.62	38.34	35.52	38.98	45.07	45.23	34.95
F_y- **DZV**	1.67	3.65	1.90	2.12	0.44	2.00	1.87	1.95
F_y- **Butterworth**	1.49	1.25	1.11	1.15	0.52	1.99	1.83	1.33
F_y - **Bessel**	1.99	1.91	1.45	1.52	0.57	2.10	1.95	1.64
F_y- **Notch**	1.62	1.84	1.25	1.37	0.32	1.73	1.57	1.39
F_z- **DZV**	1.58	5.14	1.88	2.11	0.65	14.86	13.23	5.63
F_z- **Butterworth**	0.88	2.03	1.06	1.19	0.33	14.73	13.18	4.77
F_z- **Bessel**	1.20	2.93	1.42	1.59	0.42	14.83	13.24	5.09
F_z- **Notch**	1.27	2.94	1.43	1.55	0.25	13.82	12.21	4.78

(a) Reduction in the maximum value of forces at the wing root.

	% Improvements							
Mass Case	**1**	**2**	**3**	**4**	**5**	**6**	**7**	**Average**
M_x- **DZV**	1.59	3.73	1.92	2.15	0.54	0.78	0.80	1.65
M_x- **Butterworth**	0.72	0.77	0.86	0.94	0.17	0.45	0.45	0.62
M_x- **Bessel**	1.05	1.57	1.23	1.35	0.28	0.54	0.56	0.94
M_x- **Notch**	1.26	1.85	1.40	1.50	0.09	0.18	0.29	0.94
M_y- **DZV**	3.17	4.26	1.86	2.11	0.59	0.64	0.62	1.89
M_y- **Butterworth**	1.04	1.13	0.88	0.98	0.16	0.34	0.32	0.69
M_y- **Bessel**	1.66	1.96	1.24	1.38	0.27	0.42	0.42	1.05
M_y- **Notch**	2.56	2.22	1.57	1.66	-0.47	-0.73	-0.43	0.91
M_z- **DZV**	38.78	14.76	36.03	32.01	51.61	54.87	54.86	40.42
M_z- **Butterworth**	24.44	6.45	20.92	16.21	31.38	45.83	46.09	27.33
M_z- **Bessel**	30.11	11.21	25.97	21.19	38.03	51.39	51.63	32.79
M_z- **Notch**	33.24	11.77	28.18	22.86	38.80	44.72	44.80	32.05

(b) Reduction in the maximum value of moments at the wing root.

Table A.2: Comparison of peak reduction in wing root forces and moments using the proposed DZV controller and traditional filters at various mass cases.

	% Improvements							
Mass Case	**1**	**2**	**3**	**4**	**5**	**6**	**7**	**Average**
F_x- **DZV**	61.03	18.99	54.47	48.93	74.50	56.97	56.78	53.10
F_x- **Butterworth**	36.11	15.31	31.90	28.14	42.32	59.45	60.06	39.04
F_x- **Bessel**	45.29	18.56	40.74	37.23	52.69	65.52	65.97	46.57
F_x- **Notch**	43.80	5.38	42.61	40.04	41.94	48.95	48.99	38.81
F_y- **DZV**	4.63	3.94	4.18	3.98	23.16	60.33	60.47	22.96
F_y- **Butterworth**	5.64	2.04	4.56	3.91	25.12	67.41	67.81	25.21
F_y - **Bessel**	5.98	2.60	4.89	4.32	25.20	68.68	69.12	25.83
F_y - **Notch**	5.07	2.50	4.28	3.84	23.54	54.28	54.41	21.13
F_z- **DZV**	17.25	5.56	11.16	7.98	42.90	57.67	57.55	28.58
F_z- **Butterworth**	9.33	2.91	6.10	4.31	19.81	55.30	56.20	21.99
F_z - **Bessel**	14.54	3.80	9.52	6.50	30.28	61.59	62.31	26.93
F_z - **Notch**	16.49	3.69	10.27	6.95	36.92	48.25	48.94	24.50

(a) Reduction in the total absorbed forces at the wing root due to oscillatory wing loading.

	% Improvements							
Mass Case	**1**	**2**	**3**	**4**	**5**	**6**	**7**	**Average**
M_x- **DZV**	5.89	3.78	4.13	3.68	28.35	44.62	44.23	19.24
M_x- **Butterworth**	4.33	1.14	2.33	1.63	16.88	31.11	31.82	12.75
M_x- **Bessel**	4.91	2.05	2.88	2.25	24.71	39.42	39.72	16.56
M_x- **Notch**	5.29	2.18	3.22	2.56	25.41	38.91	38.70	16.61
M_y- **DZV**	19.54	5.29	13.26	9.90	48.09	57.40	56.56	30.01
M_y- **Butterworth**	11.63	1.98	8.22	6.40	20.61	25.84	25.97	14.38
M_y- **Bessel**	16.05	3.17	11.44	8.37	31.97	37.47	37.46	20.85
M_z- **Notch**	19.28	3.47	12.70	9.09	40.58	43.65	43.65	24.63
M_z- **DZV**	63.47	43.89	61.61	59.61	64.88	65.65	65.70	60.69
M_z- **Butterworth**	61.06	37.58	56.81	53.26	62.05	74.05	74.60	59.92
M_z- **Bessel**	65.24	41.76	60.62	56.92	66.77	77.18	77.52	63.72
M_z- **Notch**	54.00	36.71	52.20	50.44	54.49	57.42	57.48	51.82

(b) Reduction in the total absorbed moments at the wing root due to oscillatory wing loading.

Table A.3: Comparison of reduction in total absorbed wing root forces and moments using the proposed DZV controller and tradition filters at various mass cases.

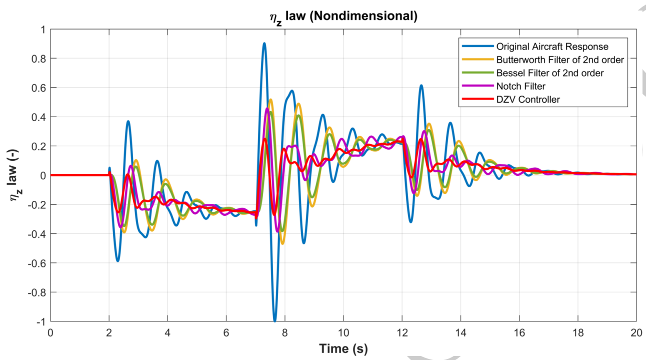

(a) η_z law response.

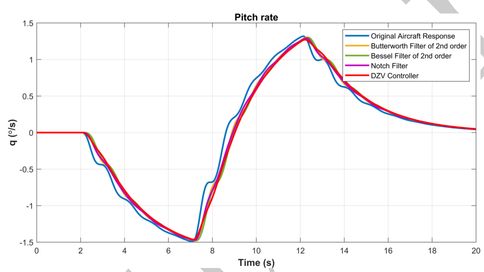

(b) Pitch rate response.

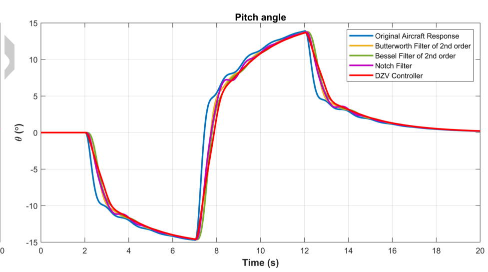

(c) Pitch angel response.

Figure A.14: Rigid body state's response for mass case 4.